Ain Shams Engineering Journal 11 (2020) 767–776

Contents lists available at ScienceDirect

Ain Shams Engineering Journal

journal homepage: www.sciencedirect.com

Engineering Physics and Mathematics

Performance evaluation of Ag/SnO_2 nanocomposite materials as coating material with high capability on antibacterial activity

Eduardo B. Tibayan Jr. [a,b], Muhammad Akhsin Muflikhun [c,d,*], Vipin Kumar [e], Christine Fisher [f], Al Rey C. Villagracia [g], Gil Nonato C. Santos [a]

[a] Physics Department, De La Salle University, 2401 Taft Avenue, Manila, Philippines
[b] College of Humanities and Sciences, De La Salle Health Sciences Institute, Lourdes E. Campos, MD Building, Dasmariñas City, Cavite, Philippines
[c] Department of Mechanical and Industrial Engineering, Faculty of Engineering, Gadjah Mada University, Jl. Grafika No.2, Yogyakarta 55281, Indonesia
[d] Graduate School of Engineering, Department of Aeronautics and Astronautics, The University of Tokyo, 7-31 Hongo, Bunkyo-ku, Tokyo 113-8656, Japan
[e] Materials Science and Technology Division (MSTD), Oak Ridge National Laboratory, Oak Ridge, TN 37830, USA
[f] Chemical Sciences Division (CSD), Oak Ridge National Laboratory (ORNL), Oak Ridge, TN 37830, USA
[g] Computational Materials Design Research Group, De La Salle University, 2401 Taft Avenue, Manila, Philippines

ARTICLE INFO

Article history:
Received 14 July 2019
Revised 23 October 2019
Accepted 28 November 2019
Available online 18 December 2019

Keywords:
Vapor deposition
Ag/SnO_2
HVPG
Antibacterial agent
DFT
Coatings

ABSTRACT

The performance of silver/tin oxide (Ag/SnO_2) nanocomposites as coating materials with high antibacterial capability is evaluated in this study. Scanning electron microscopy (SEM) and density functional theory (DFT) analyses were used to characterize the nanocomposite structures and confirm that Ag (1 1 1) and SnO_2 (1 1 0) form nanorods of Ag/SnO_2. The antibacterial properties of these materials were investigated by using an Alamar Blue Assay (ABA) absorbance method. The results indicated that toxicity to *E. coli* and *S. aureus* increased with respect to the proportion of Ag within the composite, with the highest antibacterial activity being observed at a 4:1 ratio of $Ag:SnO_2$. Additionally, the antimicrobial properties of the composites were enhanced when particle sizes were reduced from the micro- to nanometer range. Our study demonstrates that nano-Ag/SnO_2 composites are highly suitable for antibacterial coatings of glass-based materials.

1. Introduction

Metal nanocomposites and metal oxide nanocomposites demonstrate excellent physical and chemical properties and are ideal candidates for novel functional materials for many applications. Metal oxide semiconductors such as SnO_2 and ZnO are known to have excellent gas-sensing sensitivities that are selective to greenhouse gases such as CO_2 and CO. Therefore, these materials can be utilized as filters to maintain good air quality [1–3]. In addition, several studies have also reported SnO_2 alongside with ZnO as having applications in the medical field as a material with antibacterial capabilities [4–7].

It has been shown in the literature that metal oxides can be used to eradicate bacteria via electrostatic interactions that change the integrity of bacterial membranes and the generation of free radicals which are toxic to bacteria. The effectiveness of this eradication depends on many factors such as the particle size of the nanomaterials, the liquid composition in the assay, the configuration of the composites, and the presence of light and UV exposure [8,9]. Ag has been indicated as an ideal candidate to combine with SnO_2 for antibacterial coatings. The flexibility of Ag/metal oxide nanomaterials and their ability to eradicate bacteria has led to a growing interest in forming Ag/SnO_2 composites among researchers [10–12].

Many methods to grow nanocomposite materials consisting of Ag/SnO_2 have been reported. Wang et al. [13] reported that Ag/SnO_2 can be successfully synthesized using a direct electroreduction method with HCl as a catalyst. Ag/SnO_2 composite nanotubes have also been produced by an electrospinning method [14]. Moreover, Liu et al. synthesized Ag/SnO_2 using a facile hydrothermal method and an in situ reduction method [15]. Other methods such as sol-gel [5], post annealing [16], precipitation

* Corresponding author.
E-mail address: akhsin.muflikhun@ugm.ac.id (M.A. Muflikhun).

Peer review under responsibility of Ain Shams University.

Production and hosting by Elsevier

https://doi.org/10.1016/j.asej.2019.11.009
2090-4479/

combined with powder metallurgy [17], and chemical spray pyrolysis [18] have also been reported in the literature.

Although these methods can be used to synthesize Ag/SnO_2 nanocomposites with good properties, the synthesis itself often uses catalysts or additional materials that require higher safety standards due to associated environmental and health impacts. In this paper, a horizontal vapor phase growth (HVPG) technique was employed to synthesize Ag/SnO_2 nanocomposites. Previous studies show that HVPG can be used to synthesize various micro- and nano-materials such as SnO_2 [19], Ag/Ge [20], and Ag/TiO_2 [21–23]. Notably, the one-pot HVPG technique is environmentally friendly, does not require additional materials or steps in the synthetic process, and yields promising results.

Recently, nanotechnology applications for glass production have received a growing interest worldwide due to increased demand and use of larger glass areas on modern buildings and skyscrapers [24]. The use of large glass windows promotes the multiplication of bacteria and microorganisms, leaving people increasingly exposed to their harmful effects. Prolonged exposure to UVA and UVB radiation from sunlight especially during heat waves is also a big challenge for commercial architecture design [25–28].

Modified glass panes that can filter UVA and UVB light without going through the process of dyeing are essential for commercial architectural applications [29–32]. The elimination of bacteria and microbes on the surface of glass is also indicated for improved human health. This study combines both the biocidal and UV filter properties of Ag/SnO_2 nanoparticle composites to create optimal glass coatings. Here, the synthesis and fabrication of Ag/SnO_2 nanocomposites is reported, along with a density functional theory (DFT) analysis to computationally verify their respective geometries. DFT was used in this work due to the precision of this theory to calculate the chemical properties such as molecules and solids (energies, electronic structures, and binding lengths) [33].

2. Materials and methods

2.1. Preparation and synthesis of Ag/SnO_2 composites

Silver (Ag) powder of 99.9% purity containing <45 μm grain size was purchased from Sigma Aldrich. Tin oxide (SnO_2) of 99% purity with <5 μm grain size was purchased from Merck. Ag:SnO_2 mass ratios of 0:5, 1:4, 2:3, 3:2, 4:1, and 5:0 formed the composite materials with each sample having a total mass of 35 mg. Ag, SnO_2 and Ag/SnO_2 materials were synthesized using an HVPG technique, which employs a thermal synthetic method that alters the materials' phases during processing, as seen in Fig. 1.

An ultrasonic machine was used to clean the quartz tube with a closed end. The tube containing Ag and SnO_2 was attached to the Thermionic High Vacuum System (THVS) and the pressure was maintained at 10^{-6} torr. The dimensions of the quartz tube were d_{inner} = 8.5 mm, d_{outer} = 11 mm, and l = 220 mm. The Ag/SnO_2 mixtures were poured inside the quartz tube and placed horizontally inside the furnace. To create a thermal gradient within the furnace, the quartz tube was positioned one-third inside (zone 1), one-third near the opening of the furnace (zone 2), and one-third outside (zone 3) as shown in Fig. 2. The sealed quartz tube containing Ag/SnO_2 mixtures was heated for t = 6 hr at T = 800 °C with a ramp-up time of 80 min.

2.2. Characterization of Ag/SnO_2 composites

Surface analysis and elemental composition of both the Ag/SnO_2 composite materials with Ag and SnO_2 controls were performed on a JEOL SEM 5310 scanning electron microscope. Each of the three zones were measured for the characterization of all prepared nanoparticles.

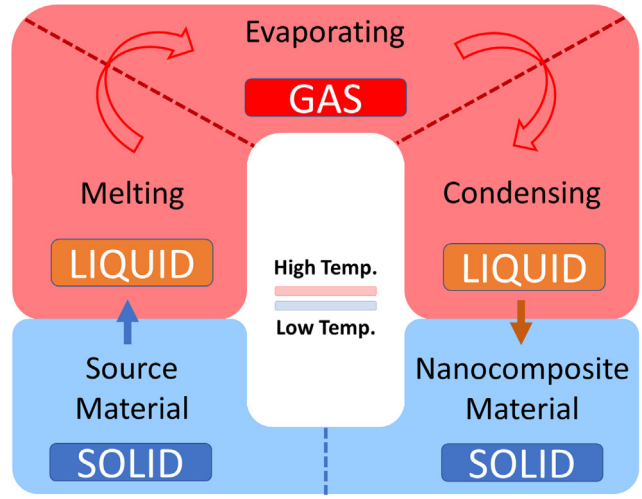

Fig. 1. HVPG induced phase conversion.

2.3. Computational assessment of Ag/SnO_2 composites via DFT

The surface structures were modelled according to the generalized gradient approximation (GGA) Functional (BLYP). BLYP functional was used in this study based on the previous research that done by Sensato et al. and Yamaguchi et al. where the DFT calculation on SnO_2 was applied. The similar model is used in this study to computationally determine the atomic geometry and electronic properties of the Ag/SnO_2 composites with the possibility to study in different theoretical descriptions which the same correlation formalism was used [34–36]. The reciprocal lattice vector for each k-point was calculated by Monkhorst Pack [37]. The k-point mesh for the bulk SnO_2 was set to 4x4x6 points while the bulk Ag was fixed to 5x5x5 points that gives satisfying results during the relaxation protocol. Computational calculations of the crystal structures and binding energies were performed using quantum chemical software DMol3. Comparisons between their structural crystalline and amorphous properties were made. DMol3 method was used due to the efficiency in numerical local orbital basis sets and it used standard molecular calculations by using arithmetic operations which can be lowered by using reciprocal space method [38]. The parameters that used in this study are listed as follow: Energy cut-off: 400 eV, Convergence criteria: 10E-5, and maximum SCF: 500.

2.4. Antibacterial testing

Two-part antibacterial tests were implemented to determine the effectiveness of the nanomaterials against bacteria. The first test involved the absorbance measurement of the turbidity of the bacterial solutions exposed to different nanomaterial mixtures. Using the Perkin Elmer UV/Vis Spectrophotometer Lambda 25, absorbance at λ = 600 nm was measured for solutions of *Escherichia coli* and *Staphylococcus aureus* [39,40]. High turbidity indicates an increase in the colony forming unit (cfu) of bacteria and results in higher absorbance wavelength values as light is scattered by the presence of microorganisms. Composites of Ag and SnO_2 with different mass ratios were collected from the three zones of the quartz tubes and added to test tubes containing a solution of nutrient broth and bacteria. Powder Ag and SnO_2 were also added to test the antibacterial effectiveness between bulk and nanomaterials.

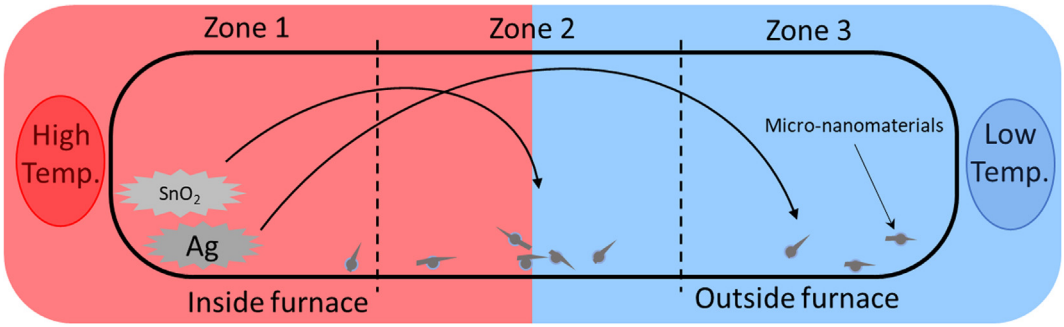

Fig. 2. Cross-sectional diagram of the furnace during the heating of the quartz tube sectioned into three equal segments: zones 1, 2 and 3 [34].

The second test used an Alamar Blue Assay (ABA) technique for quantitative analysis. The proliferation from cell lines of human, animal, bacteria and fungi samples were studied. ABA methods incorporate a fluorometric or calometric indicator to detect metabolic activity. Fluorescence and color changes occur in response to reduction-oxidation reactions within mediums containing cell growth. The active ingredient of ABA, Resazurin, is reduced from its blue, non-fluorescent form into red, fluorescent Toresorufin after successfully permeating a viable cell. ABA techniques have several advantages over existing testing methods, such as non-toxicity, ease of application, and non-interference with cell metabolism. In our set-up, 500 μL of Ag/SnO_2 composites and powder Ag + SnO_2 solutions were transferred to sterilized test tubes, followed by the addition of 50 μL ABA to form a 10:1 ratio. The test tubes containing the solution-reagent mixtures were incubated at 37 °C and monitored for color changes 12 and 24 hr after incubation. Color changes from the original blue color of ABA were used as indicators of the presence of viable cfu bacteria within the mixture.

3. Results and discussion

3.1. SEM imaging

A summary of the surface morphologies of Ag, SnO_2, and Ag/SnO_2 composite materials and bulk SnO_2 and Ag powders is shown in Fig. 3. Three different zones across the temperature gradient of the quartz tubes are examined. The SEM micrographs depict the presence of randomly oriented nanowires, nanofibers, nanospheres and nanocotton-like structures. The representative EDX analysis from Ag/SnO_2 nanocomposite material where the ratio between Ag:SnO_2 is 1:4 can be seen in Fig. 4. The results show that since the synthesis of nanocomposites process occurred in the vacuum

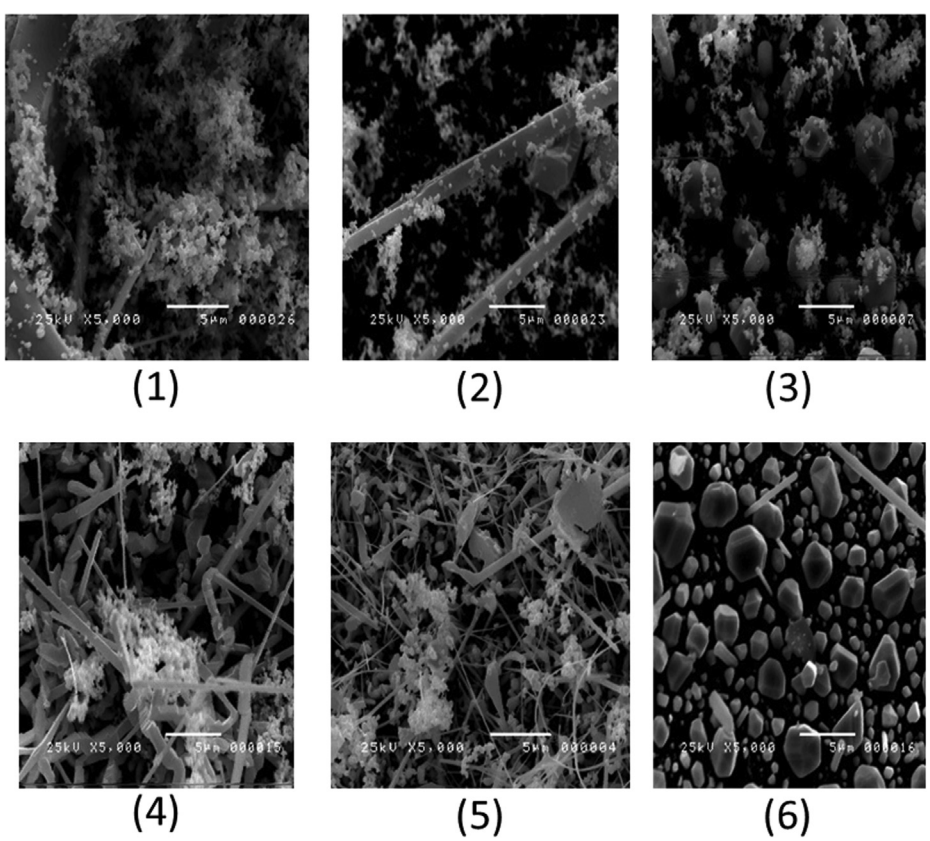

Fig. 3. Representative SEM images of Ag/SnO_2 in Ag:SnO_2 mass ratios of (1) 0:5, (2) 1:4, (3) 2:3, (4) 3:2, (5) 4:1, (6) 5:0.

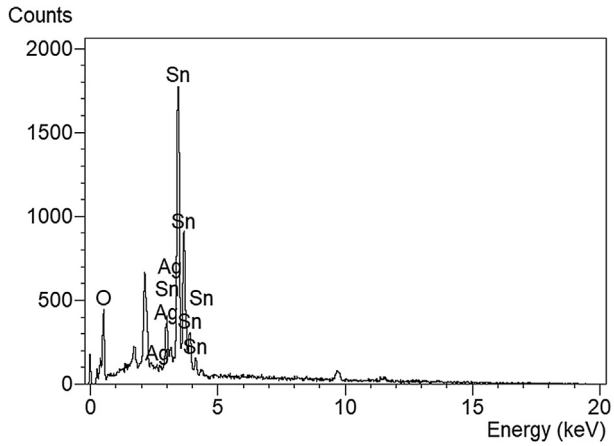

Fig. 4. EDX spectrum of Ag/SnO_2 nanocomposite material with ratio 1:4.

condition, the result from EDX show both Ag, Sn, and O are the element that have high intensity. The absence of the other element are the prove that HVPG technique are capable to synthesis nanomaterial with high purity.

Most nanomaterials are observed in zone 3 while zone 1 and zone 2 display structures ranging from nanometer to micrometer size. Two different types of growth mechanisms can potentially explain the deposition of nanomaterials found in each zone. In the first growth mechanism, the source material is initially found in zone 1. It receives heat from its surroundings, acting as an agent of heat transfer and undergoing a phase transition from solid to gas for effective spreading. The convective motion of gases inside the quartz tube influences the existing longitudinal thermal gradient of tube, making any material accumulation or deposition impossible. The source powder is likely vaporized from zone 1 and 3, but a possible phase transition from vapor to liquid can occur as vapor traverses from zone 1 to 2. Thus, nanostructures are formed by the process of creep flow and cooling after the dwell time of 6 hr.

The second type of growth mechanism involves the formation of SnO_2 nanowires as explained by Bhardwaj et al. [41]. Because Sn has a low melting point, the deposited Sn nanoparticles are likely converted into liquid nanodroplets which induce self-catalytic growth of SnO_2 nanowires. As the Ag content of the source material increases, Ag nanoparticles form and dissolve Sn, thereby creating Ag-Sn eutectic nanodroplets. Functioning as a catalyst, the Ag-Sn eutectic nanodroplets dissolve incoming Sn, O and Ag atoms. Due to the temperature-gradient-driven supersaturation, precipitation of Ag, Sn and O follows the formation of SnO_2 nanowires. A further increase in Ag concentration results in the creation of Ag_3Sn alloy nanodroplets which dissolve any inbound Sn, O and Ag atoms from the vapor phase, inducing the formation of SnO_2 nanowires. The initial growth of SnO_2 nanowires produces a deposition site for Sn and Ag nanoparticles in the vapor phase, where Ag_3Sn alloy nanodroplets can grow as secondary nucleation centers for SnO_2 nanowire formation in a self-catalytic cycle. These secondary nucleation centers then create bridged interconnections between discrete SnO_2 nanowires.

3.2. DFT analysis

3.2.1. SnO_2 surface structure

SnO_2(1 1 0) is considered a thermodynamically and electrostatically stable material with a predominantly crystal face surface since the [1 0 0] plane has the least surface energy relative to other orientations [42,43]. This plane consists of O and Sn atoms separated by planes containing only O atoms which can be written as O–Sn_2O_2–O, with ionic charges of 2-, 4+ and 2-, respectively [43]. At the surface, the two outermost layers of O are called "bridging" oxygen atoms such that removing one O creates a "bridging vacancy." The lattice constants are calculated to be a = 4.84 Å, b = 3.28 Å and c = 18.0 Å for both single- and double-unit cells, which is in close agreement with a study carried out by Habgood and Harrison [44]. Fig. 5. illustrates the SnO_2(1 1 0) crystal and band structures and the density of states for a double-unit cell, with computed band gaps of 3.73 eV (332.63 nm). Based on the calculated band gap energies, the SnO_2(1 1 0) surface structure is a good candidate for UVB and UVC ray absorption.

3.2.2. SnO_2 (1 1 0) on Ag (1 1 1) surface structure

SnO_2 (1 1 0) on Ag (1 1 1) was analyzed according to a bottom-top termination along the surface in order to determine the

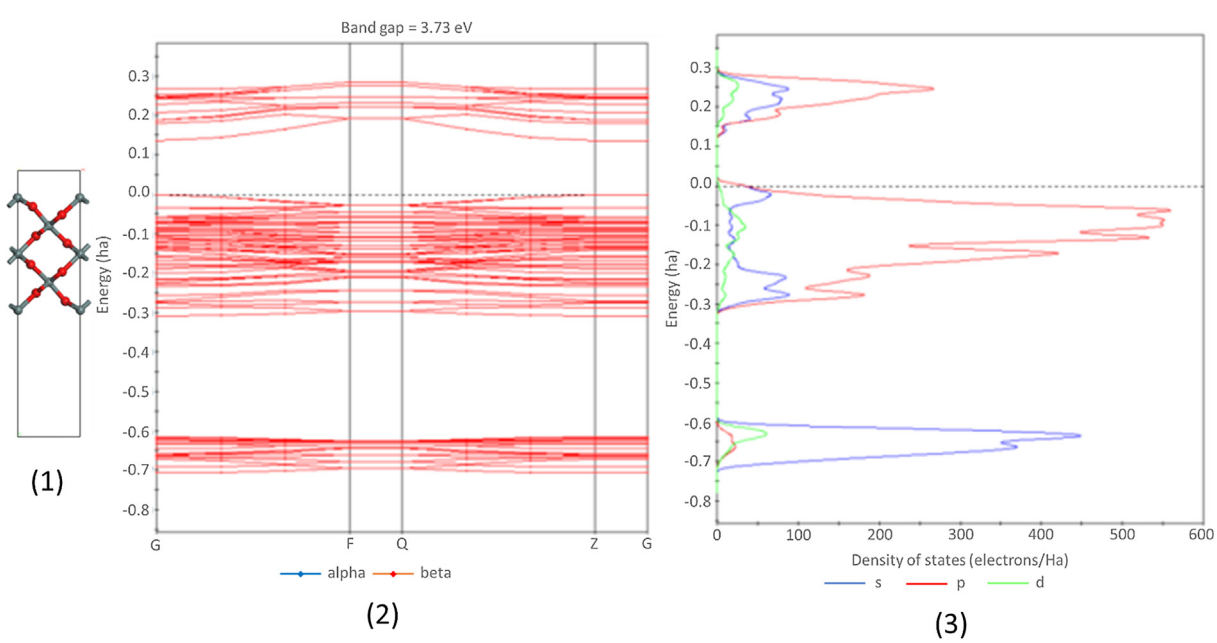

Fig. 5. SnO_2 (1 1 0) (1) Crystal Structure, (2) Band Structure, and (3) Density of States.

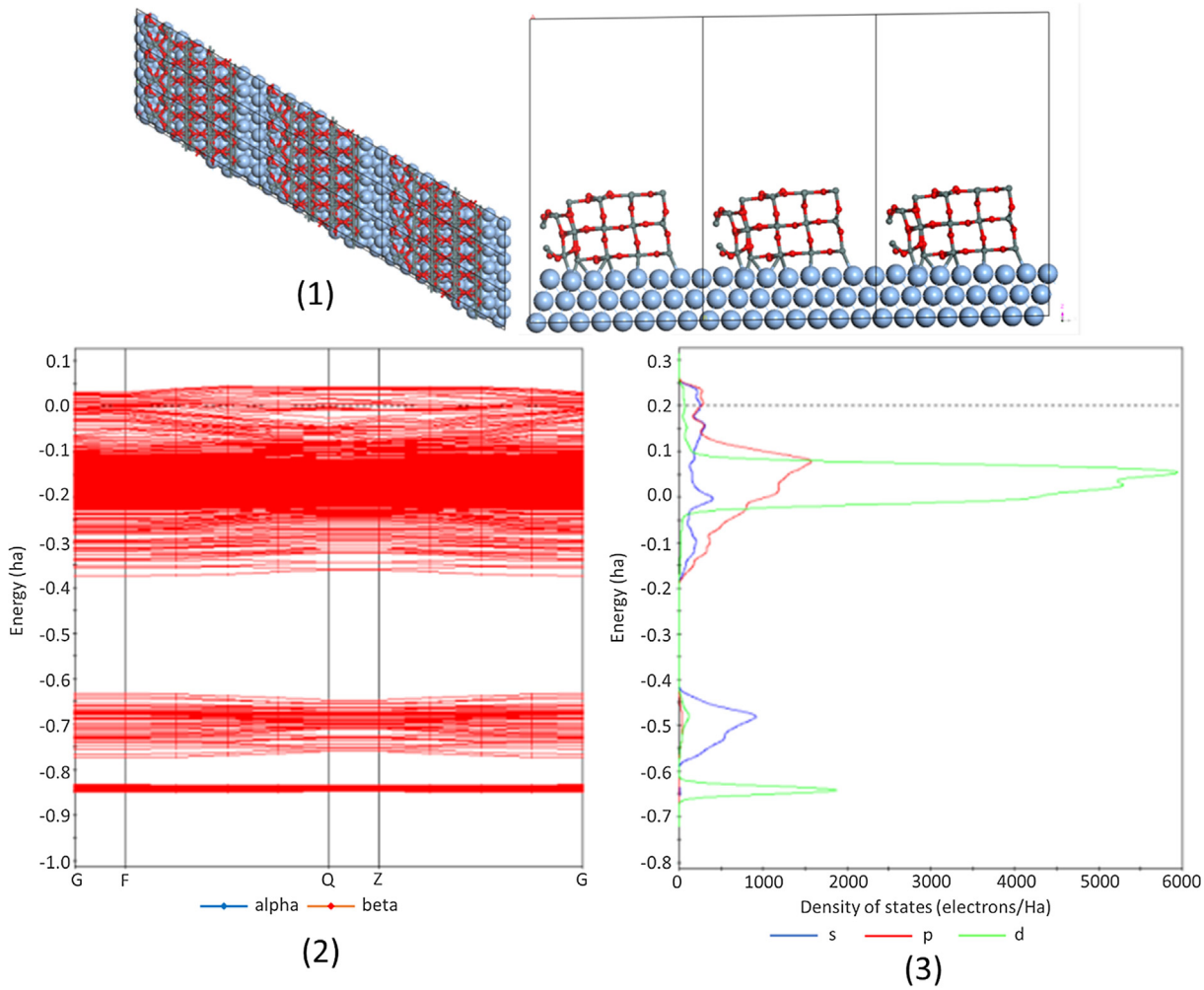

Fig. 6. (1) SnO_2(1 1 0) on Ag(1 1 1) Crystal Structure, (2) Band Structure, and (3) Density of States for larger unit cells on SnO_2 Nanorods over a silver surface.

geometric and electronic structure of the Ag/SnO_2 composite. The unit cell, SnO_2 atoms, and first layer of Ag (1 1 1) are relaxed, whereas the bottom layer of Ag (1 1 1) is fixed. The computed lattice constants are a = 5.45 Å, b = 6.31 Å, and c = 18 Å. Fig. 5. shows the crystal structures of SnO_2 (1 1 0) on Ag (1 1 1) for possible atomic termination combinations. The lowest band gap is found at the Sn—Sn termination while the highest band gaps are calculated at the O—Sn and O—O terminations.

The geometric crystal structure for SnO_2 nanorods using Ag surfaces is shown in Fig. 6, along with the corresponding band structure and density of states. These computational results are experimentally supported by the SEM images where SnO_2 nanorods were attached to the Ag nanoparticles. A direct experimental comparison for this computational model can be made with a report done by Kim et al. [45] where the [1 0 0] facets were seen to be prominent in SnO_2 nanorods synthesized at 1200 K by thermal evaporation. The results suggest the direct increase of the relative intensity of [1 0 0] facets as O partial pressure increases simultaneously.

3.3. Antibacterial properties of Ag/SnO_2 nanoparticles

3.3.1. Antibacterial effect on E. Coli

The change or retention of color within ABA solutions indicates the proliferation or abatement of *E. coli* after incubation, respectively. Fig. 7. shows the biocidal effect of nanomaterial mixtures with *E. coli* 12 hr after incubation. Samples that indicated color changes are *E. coli* (+control), *E. coli* with SnO_2 bulk powder, and *E. coli* with Ag bulk powder, revealing that *E. coli* remains viable when exposed to the larger, powdered forms of pure Ag and SnO_2. As *E. coli* continues to grow, the innate metabolic activity of the bacteria results in the chemical reduction of AB (alamarBlue), causing the redox indicator to change from the oxidized (non-fluorescent blue) form to the reduced (fluorescent red) form. When AB is added to cell cultures, the oxidized AB enters the cytosol and is converted to its reduced form via accepting electrons from mitochondrial enzymes, including cytochromes, NADPH, FADH, FMNH and NADH. This redox reaction is accompanied by a shift of the culture medium from indigo blue to fluorescent pink [46–48].

After 24 hr of incubation, a shift from pink to orange is observed on both the Ag and SnO_2 powders with *E. coli* as shown in Fig. 8. A halt to the spread of *E. coli* cells may have caused the change of color due to either a high cell population or extended incubation time. However, there was no remarkable difference in the color of *E. coli* solutions with the Ag/SnO_2 composite and bulk nanomaterials. Based on these observations, the effectiveness of the composite against *E. coli* is proportional to the reduction of theAg/SnO_2 composite particle size. The absorbance values presented in Table 1 show that the intensity decreased after 12 hr and further reduced after 24 hr, thereby indicating the eradication of *E. coli* due to prolonged exposure to the nanomaterial

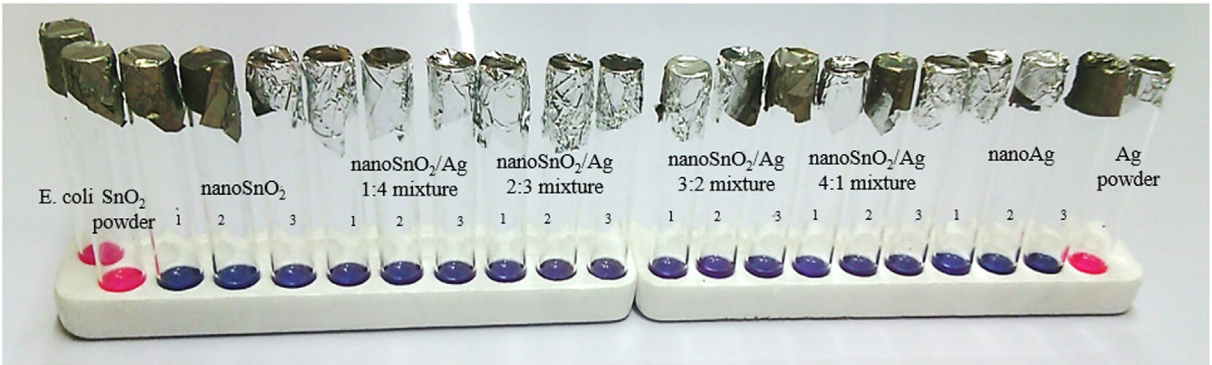

Fig. 7. ABA/*E. coli* after 12 hr of incubation.

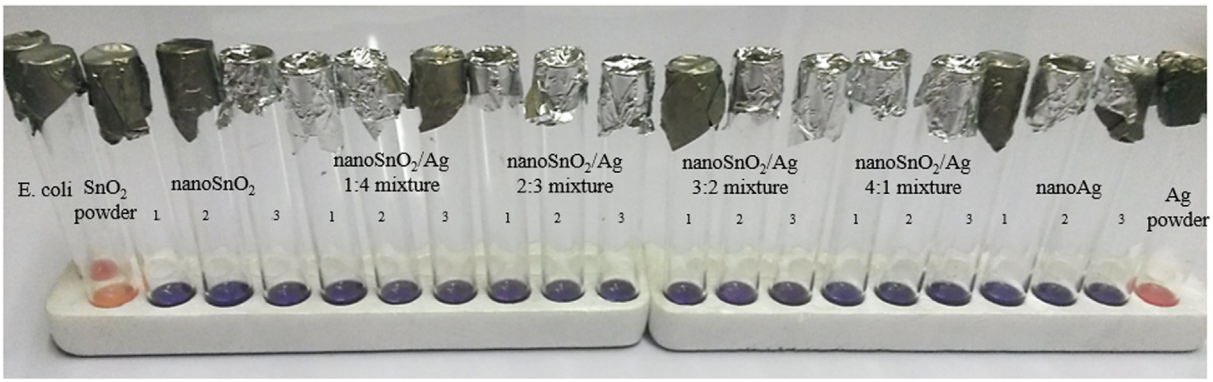

Fig. 8. ABA/E. Coli after 24 hr of incubation.

Table 1
Absorbance values of E. Coli at 600 nm.

Wavelength	600 nm				
Samples	0 h	12 h	$A_{12h} - A_{0h}$	24 h	$A_{24h} - A_{12h}$
***E. Coli*, no material**	0.559	0.629	0.07	0.626	−0.003
SnO_2 powder	2.071	2.125	0.054	2.12	−0.005
SnO_2 nanomaterial zone 1	1.921	1.915	−0.006	1.893	−0.022
SnO_2 nanomaterial zone 2	1.896	1.889	−0.007	1.863	−0.026
SnO_2 nanomaterial zone 3	2.081	2.078	−0.003	2.047	−0.031
Ag/SnO_2 1:4 zone 1	1.356	1.341	−0.015	1.304	−0.037
Ag/SnO_2 1:4 zone 2	1.392	1.38	−0.012	1.337	−0.043
Ag/SnO_2 1:4 zone 3	1.426	1.407	−0.019	1.354	−0.053
Ag/SnO_2 2:3 zone 1	1.262	1.244	−0.018	1.191	−0.053
Ag/SnO_2 2:3 zone 2	1.388	1.364	−0.024	1.31	−0.054
Ag/SnO_2 2:3 zone 3	1.348	1.319	−0.029	1.26	−0.059
Ag/SnO_2 3:2 zone 1	1.199	1.168	−0.031	1.111	−0.057
Ag/SnO_2 3:2 zone 2	1.264	1.236	−0.028	1.178	−0.058
Ag/SnO_2 3:2 zone 3	1.216	1.174	−0.042	1.111	−0.063
Ag/SnO_2 4:1 zone 1	0.962	0.904	−0.058	0.823	−0.081
Ag/SnO_2 4:1 zone 2	1.144	1.083	−0.061	0.998	−0.085
Ag/SnO_2 4:1 zone 3	1.138	1.068	−0.07	0.954	−0.114
Ag nanomaterial zone 1	0.645	0.589	−0.056	0.512	−0.077
Ag nanomaterial zone 2	0.687	0.625	−0.062	0.542	−0.083
Ag nanomaterial zone 3	0.996	0.932	−0.064	0.839	−0.093
Ag powder	0.628	0.668	0.04	0.657	−0.011

mixtures. Furthermore, the amount of Ag in the mixture is inversely proportional to its absorbance, confirming its effectiveness as an antibacterial agent. Since Ag is a natural biocidal material, the toxicity of a solution of *E. coli* is improved with an increased presence of Ag within Ag/SnO_2 mixtures [49,50].

A possible explanation for the elimination of the *E. coli* within Ag/SnO_2 solutions, determined from absorbance measurements, is due to the nanomaterial's breaking of the bacterial cell wall. Since the subsequently leaked cytoplasmic material is composed of soluble proteins, salts, and small molecules, these components do not contribute to light scattering and in contrast, would result in a decrease of the optical or absorbance intensity of the sample. Moreover, reformed cells would be smaller and scatter less light which results in a lower absorbance as shown in Table 1.

3.3.2. Antibacterial effect on S. Aureus

The biocidal effect of SnO_2 and Ag bulk, powder and composite nanomaterials were further tested on the bacteria *Staphylococcus aureus* (*S. aureus*). After 12 hr of incubation, only two of the samples, *S. aureus* (+control) and SnO_2 powder with *S. aureus*, demonstrated a color change, indicating no effect on the elimination of *S. aureus*, depicted in Fig. 9. Further incubation to 24 hr revealed that SnO_2 nanoparticles and Zone 1-harvested Ag nanomaterials are also ineffective as antibacterial agents against *S. aureus* as illustrated in Fig. 10. Both the powdered and nanoparticle forms of SnO_2 are viable agents against the *S. aureus* solution. However, nanocomposites of Ag/SnO_2 prove to be a consistently effective antibacterial material on both *E. coli* and *S. aureus*. Thus, nano-sized materials have a higher toxicity towards these bacteria compared to their powdered forms, which is consistent with the results found by previous studies [50,51].

The absorbance intensity decreased for all solutions after a 12 hr incubation period except for the *S. aureus* control, as presented in Table 2. For the case of *S. aureus*, the inhibitory action of the Ag/SnO_2 composite can be tied to the respiration of the bac-

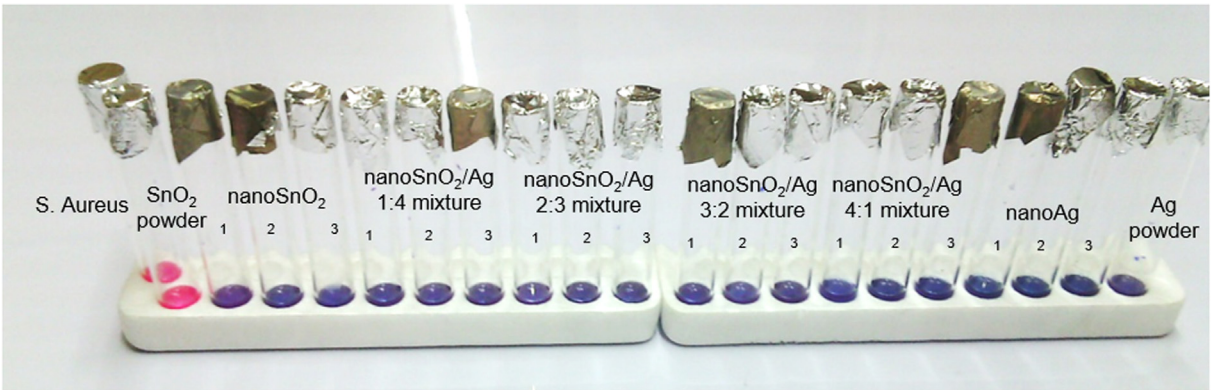

Fig. 9. ABA/S. Aureus after 12 hr of incubation.

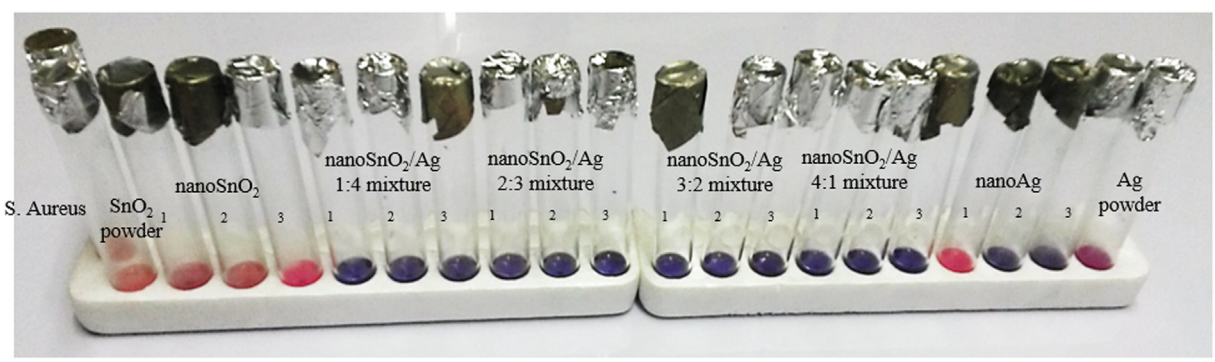

Fig. 10. ABA /S. Aureus after 24 hr of incubation.

Table 2
Absorbance values of S. aureus at 600 nm.

Wavelength Samples	600 nm 0 h	12 h	$A_{12h} - A_{0h}$	24 h	$A_{24h} - A_{12h}$
***S. aureus*, no material**	0.208	0.316	0.108	0.425	0.109
SnO_2 powder	1.968	2.069	0.101	2.176	0.107
SnO_2 nanomaterial zone 1	1.741	1.812	0.071	1.871	0.059
SnO_2 nanomaterial zone 2	1.67	1.697	0.027	1.769	0.072
SnO_2 nanomaterial zone 3	1.418	1.452	0.034	1.554	0.102
Ag/SnO_2 1:4 zone 1	1.581	1.575	−0.006	1.539	−0.036
Ag/SnO_2 1:4 zone 2	1.595	1.42	−0.175	1.354	−0.066
Ag/SnO_2 1:4 zone 3	1.567	1.403	−0.164	1.327	−0.076
Ag/SnO_2 2:3 zone 1	1.444	1.229	−0.215	1.144	−0.085
Ag/SnO_2 2:3 zone 2	1.414	1.388	−0.026	1.334	−0.054
Ag/SnO_2 2:3 zone 3	1.473	1.225	−0.248	1.129	−0.096
Ag/SnO_2 3:2 zone 1	1.331	1.117	−0.214	1.035	−0.082
Ag/SnO_2 3:2 zone 2	1.366	1.261	−0.105	1.169	−0.092
Ag/SnO_2 3:2 zone 3	1.411	1.192	−0.219	1.092	−0.100
Ag/SnO_2 4:1 zone 1	1.292	1.087	−0.205	0.995	−0.092
Ag/SnO_2 4:1 zone 2	1.309	1.146	−0.163	1.013	−0.133
Ag/SnO_2 4:1 zone 3	1.403	1.157	−0.246	1.008	−0.149
Ag nanomaterial zone 1	0.635	0.617	−0.018	0.727	0.110
Ag nanomaterial zone 2	0.776	0.59	−0.186	0.492	−0.098
Ag nanomaterial zone 3	1.069	0.896	−0.173	0.786	−0.110
Ag powder	0.687	0.734	0.047	0.802	0.048

teria and the corresponding change in turbidity, as stated by Avidor et al. [52]. Furthermore, previous studies show that nanoparticles' toxicity mechanism depends on the composition, surface modification, intrinsic properties and type of bacteria species.

Nanoparticles can either penetrate the bacterial cell wall and bind to the phospholipid layer of the cytoplasmic membrane, bind to the DNA of the bacteria and disrupt its replication, or impair the ability of the ribosome to transcribe RNA or bind to the sulfhydryl group of the cytochrome [53]. Although the exact mechanism remains unknown, our experimental results recapitulate that reducing the size of the Ag/SnO_2 composites to the nanoparticle range proves to be effectively toxic to both *E. coli* and *S. aureus* bacteria.

4. Conclusion

Ag/SnO_2 nanocomposite materials were successfully synthesized using a simple HVPG technique which resulted in high purity results, an eco-friendly synthesis, and a low cost of production. The SEM images indicated that the morphology of Ag/SnO_2 composites changed with respect to the ratio of starting materials, which is reflected in the absorbance data and subsequent antibacterial capabilities. This study shows various nanomaterials were successfully synthesized including wires, rods, spheres and cotton-like composites from the three zone areas of the quartz tube. DFT analysis using the quantum chemical software DMol3 illustrates that the computed band gap energy of Ag (1 1 1) matches the SnO_2 (1 1 0) surfaces, supporting the experimental findings.

The ABA technique demonstrates that Ag/SnO_2 composites are toxic to both *E. coli* and *S. aureus* bacteria. The ABA indicator induced color changes when exposed to powered macromaterials of Ag and SnO_2, revealing the proliferation of bacteria within these mediums. However, color shifts were not seen within the Ag/SnO_2 composites that were both nanosized and contained high ratios of Ag:SnO_2, suggesting that these materials are highly capable as antibacterial agents. These results confirm that antibacterial properties are enhanced in nanoparticles and suggest that Ag/SnO_2 nanocomposite materials are suitable for coating applications with a high performance in antibacterial activity. Based on the results, this material can be applied in residential and commercial glass windows along with glass-based materials that are exposed to UV light. Additionally, medical applications have yet to be explored but the present results are promising for the production of materials with highly antimicrobial properties against both gram-positive and gram-negative bacteria.

Acknowledgements

The authors would like to thank DLSHSI, College of Humanities and Sciences for allowing the authors to perform the antibacterial experiments in the microbiology and chemistry laboratory, as well as Gwen Castillon, Prane Ong, and Rey Coria from the DLSU Solid State Physics Laboratory for their assistance and guidance during the experimental works. Dr. Vipin Kumar was supported by the U.S. Department of Energy, Office of Energy Efficiency and Renewable Energy, Advanced Manufacturing Office, under contract DE-AC05-00OR22725 with UT-Battelle, LLC.

References

[1] Ge S, Zheng H, Sun Y, Jin Z, Shan J. Ag/SnO2/graphene ternary nanocomposites and their sensing properties to volatile organic compounds. J Alloy Compd 2016;659:127–31. doi: https://doi.org/10.1016/j.jallcom.2015.11.046.
[2] Maldonado A, Olvera MDL. Gas-sensing characteristics of undoped-SnO2 thin films and Ag/SnO2 and SnO2/Ag structures in a propane atmosphere. Mater Charact 2007;58:740–4. doi: https://doi.org/10.1016/j.matchar.2006.11.016.
[3] Shypylenko A, Pshyk AV, Grześkowiak B, Medjanik K, Peplinska B, Oyoshi K, et al. Effect of ion implantation on the physical and mechanical properties of Ti-Si-N multifunctional coatings for biomedical applications. Mater Des 2016;110:821–9. doi: https://doi.org/10.1016/j.matdes.2016.08.050.
[4] Paraguay-delgado F, Orrantia-borunda E, Ch A, Luna-velasco A. Chemosphere Size effect of SnO2 nanoparticles on bacteria toxicity and their membrane damage 2016;165:33–40. doi: https://doi.org/10.1016/j.chemosphere.2016.09.003.
[5] Kumar K, Kumar P, Kumar V, Harris RA, Kroon RE, Viljoen B, et al. Synthesis and evaluation of optical and antimicrobial properties of Ag-SnO 2 nanocomposites. Phys B Phys Condensed Matter 2018;535:338–43. doi: https://doi.org/10.1016/j.physb.2017.08.028.
[6] Turlybekuly A, Pogrebnjak AD, Sukhodub LF, Sukhodub LB, Kistaubayeva AS, Savitskaya IS, et al. Synthesis, characterization, in vitro biocompatibility and antibacterial properties study of nanocomposite materials based on hydroxyapatite-biphasic ZnO micro- and nanoparticles embedded in Alginate matrix. Mater Sci Eng C 2019;104:109965. doi: https://doi.org/10.1016/j.msec.2019.109965.
[7] Pogrebnjak A, Sukhodub L, Sukhodub L, Bondar O, Kumeda M, Shaimardanova B, et al. Composite material with nanoscale architecture based on bioapatite, sodium alginate and ZnO microparticles. Ceram Int 2019;45:7504–14. doi: https://doi.org/10.1016/j.ceramint.2019.01.043.
[8] John N, Somaraj M, Tharayil NJ. Science direct synthesis, characterization and anti - bacterial activities of pure and Ag - doped SnO 2 Nanoparticles. Mater Today: Proc 2017;4:4351–7. doi: https://doi.org/10.1016/j.matpr.2017.04.005.
[9] Duan Z, Deng L, Shi Z, Zhang H, Zeng H, Crittenden J. In situ growth of Ag-SnO2 quantum dots on silver phosphate for photocatalytic degradation of carbamazepine : performance, mechanism and intermediates toxicity assessment. J. Coll. Interf. Sci. 2019;534:270–8. doi: https://doi.org/10.1016/j.jcis.2018.09.039.
[10] Wang J, Wang C, Kang Y. The effects of annealing treatment on microstructure and contact resistance properties of cold sprayed Ag-SnO 2 coating. J Alloy Compd 2017;714:698–703. doi: https://doi.org/10.1016/j.jallcom.2017.04.227.
[11] Li H, He Y, Jin P, Cao Y, Fan M, Zou X, et al. Highly selective detection of trace hydrogen against CO and CH 4 by Ag / Ag 2 O – SnO 2 composite microstructures. Sens Actuat. B 2016;228:515–22. doi: https://doi.org/10.1016/j.snb.2016.01.078.
[12] Muflikhun MA, Chua AY, Santos GNC. Statistical design analysis of silver-titanium dioxide nanocomposite materials synthesized via horizontal vapor phase growth (HVPG). Key Eng Mater 2017;735:210–4. doi:10.4028/www.scientific.net/KEM.735.210.
[13] Wang X, Xiao W, Zhang J, Wang Z, Jin X. Electrochemistry communications nanoporous Ag-Sn derived from codeposited AgCl-SnO2 for the electrocatalytic reduction of CO2 with high formate selectivity. Electrochem Commun 2019;102:52–6. doi: https://doi.org/10.1016/j.elecom.2019.03.017.
[14] Miao Y, He S, Zhong Y, Yang Z, Weei W, Liu T. Electrochimica Acta A novel hydrogen peroxide sensor based on Ag/SnO2 composite nanotubes by electrospinning. Electrochimica Acta 2013;99:117–23. doi: https://doi.org/10.1016/j.electacta.2013.03.063.
[15] Liu D, Pan J, Tang J, Liu W, Bai S, Luo R. Journal of physics and chemistry of solids Ag decorated SnO2 nanoparticles to enhance formaldehyde sensing properties. J. Phys. Chem. Solids 2019;124:36–43. doi: https://doi.org/10.1016/j.jpcs.2018.08.028.
[16] Zhao J, Deng R, Qin J, Song J, Jiang D, Yao B, et al. Photoresponse enhancement in SnO2 -based ultraviolet photodetectors via coupling with surface plasmons of Ag particles. J Alloy Compd 2018;748:398–403. doi: https://doi.org/10.1016/j.jallcom.2018.03.180.
[17] Li G, Cui H, Chen J, Fang X, Feng W, Liu J. Formation and effects of CuO nanoparticles on Ag/SnO2 electrical contact materials. J Alloy Compd 2017;696:1228–34. doi: https://doi.org/10.1016/j.jallcom.2016.12.092.
[18] Kolhe PS, Koinkar PM, Maiti N, Sonawane KM. Synthesis of Ag doped SnO2 thin fi lms for the evaluation of H2S gas sensing properties. Physica B: Phys Condensed Matter 2017;524:90–6. doi: https://doi.org/10.1016/j.physb.2017.07.056.
[19] Briones JC, Castillon G, Delmo MP, Santos GNC. Magnetic-field-enhanced morphology of tin oxide nanomaterials for gas sensing 2017 Applications. J. Nanomater. 2017. doi: https://doi.org/10.1155/2017/4396723.
[20] Muflikhun MA, Castillon GB, Santos GNC, Chua AY. Micro and Nano Silver-Graphene Composite Manufacturing via Horizontal Vapor Phase Growth (HVPG) Technique. Mater. Sci. Forum 2017;901:3–7. 10.4028/www.scientific.net/msf.901.3.
[21] Muflikhun MA, Frommelt MC, Farman M, Chua AY. Santos GNC. Structures, mechanical properties and antibacterial activity of Ag/TiO2 nanocomposite materials synthesized via HVPG technique for coating application. Heliyon 2019;5. 1–21 10.1016/j.heliyon.2019.e01475.
[22] Muflikhun MA, Santos GN, Chua AY. Synthesis and characterization of silver-titanium nanocomposite via horizontal vapor phase growth (HVPG) technique. DLSU Res Congress 2015:1–5.
[23] Muflikhun MA, Chua AY, Santos GNC. Structures, morphological control, and antibacterial performance of ag/TiO2 nanocomposite materials. Adv Mater Sci Eng 2019 2019. doi: https://doi.org/10.1155/2019/9821535.
[24] Jelle BP, Gustavsen A, Nilsen TN, Jacobsen T. Solar material protection factor (SMPF) and solar skin protection factor (SSPF) for window panes and other glass structures in buildings. Sol Energy Mater Sol Cells 2007;91:342–54. doi: https://doi.org/10.1016/j.solmat.2006.10.017.
[25] Skarstad K, Steen HB, Boye E. Cell cycle parameters of slowly growing Escherichia coli B/r studied by flow cytometry. J Bacteriol 1983;154:656–62.

[26] Leadbetter ER, Poindexter JS. Methods and special applications in bacterial ecology. Springer Science & Business Media; 1986.
[27] Damiani E, Rosati L, Castagna R, Carloni P, Greci L. Changes in ultraviolet absorbance and hence in protective efficacy against lipid peroxidation of organic sunscreens after UVA irradiation. J Photochem Photobiol B 2006;82. doi: https://doi.org/10.1016/j.jphotobiol.2005.03.011.
[28] Matsumura Y, Ananthaswamy HN. Toxic effects of ultraviolet radiation on the skin. Toxicol Appl Pharmacol 2004;195:298–308.
[29] deRichter R, Caillol S. Fighting global warming: The potential of photocatalysis against CO2, CH4, N2O, CFCs, tropospheric O3, BC and other major contributors to climate change. J Photochem Photobiol C 2011;12:1–19. doi: https://doi.org/10.1016/j.jphotochemrev.2011.05.002.
[30] Babu B, Cho M, Byon C, Shim J. One pot synthesis of Ag-SnO2 quantum dots for highly enhanced sunlight-driven photocatalytic activity. J Alloy Compd 2018;731:162–71. doi: https://doi.org/10.1016/j.jallcom.2017.10.011.
[31] Natarajan TS, Natarajan K, Bajaj HC, Tayade RJ. Study on identification of leather industry wastewater constituents and its photocatalytic treatment. Int J Environ Sci Technol 2013;10:855–64. doi: https://doi.org/10.1007/s13762-013-0200-9.
[32] Tuchinda C, Srivannaboon S, Lim HW. Photoprotection by window glass, automobile glass, and sunglasses. J Am Acad Dermatol 2006;54:845–54. doi: https://doi.org/10.1016/j.jaad.2005.11.1082.
[33] Parr R. [Robert_G._Parr,_Yang_Weitao]_Density-functional_t(z-lib.org).pdf. Oxford University Press; 1989.
[34] Lenglet M. Iono-covalent character of the metal-oxygen bonds in oxides: A comparison of experimental and theoretical data. Act Passive Electron Compon 2004;27:1–60. doi: https://doi.org/10.1080/0882751031000116142.
[35] Sensato FR, Custódio R, Calatayud M, Beltrán A, Andrés J, Sambrano JR, et al. Periodic study on the structural and electronic properties of bulk, oxidized and reduced SnO2(1 1 0) surfaces and the interaction with O2. Surf Sci 2002;511:408–20. doi: https://doi.org/10.1016/S0039-6028(02)01542-X.
[36] Yamaguchi Y, Nagasawa Y, Shimomura S, Tabata K, Suzuki E. A density functional theory study of the interaction of oxygen with a reduced SnO2 (110) surface. Chem Phys Lett 2000;316:477–82. doi: https://doi.org/10.1016/S0009-2614(99)01365-2.
[37] Pack JD, Monkhorst HJ. Special points for Brillouin-zone integrations"-a reply. Phys Rev B 1977;16:1748–9. doi: https://doi.org/10.1103/PhysRevB.16.1748.
[38] Delley B. Time dependent density functional theory with DMol3. J Phys: Condens Matter 2010;22.. doi: https://doi.org/10.1088/0953-8984/22/38/384208.
[39] El-Shanshoury AE-RR, ElSilk SE, Ebeid ME. Extracellular biosynthesis of silver nanoparticles using escherichia coli ATCC 8739, bacillus subtilis ATCC 6633, and streptococcus thermophilus ESh1 and their antimicrobial activities. ISRN Nanotechnology 2011;2011:1–7. doi: https://doi.org/10.5402/2011/385480.
[40] McBirney SE, Trinh K, Wong-Beringer A, Armani AM. Wavelength-normalized spectroscopic analysis of Staphylococcus aureus and Pseudomonas aeruginosa growth rates. Biomed Opt Exp 2016;7:4034. doi: https://doi.org/10.1364/boe.7.004034.
[41] Bhardwaj N, Kuriakose S, Mohapatra S. Structural and optical properties of SnO2 nanotowers and interconnected nanowires prepared by carbothermal reduction method. J Alloy Compd 2014;592:238–43.
[42] Batzill M, Diebold U. The surface and materials science of tin oxide. Prog Surf Sci 2005;79:47–154. doi: https://doi.org/10.1016/j.progsurf.2005.09.002.
[43] Floriano EA, Scalvi LV, Sambrano JR, Geraldo V. Evaluation of bulk and surfaces absorption edge energy of sol-gel-dip-coating SnO2 thin films. Mater Res 2010;13:437–43.
[44] Habgood M, Harrison N. An ab initio study of oxygen adsorption on tin dioxide. Surf Sci 2008;602:1072–9.
[45] Kim HW, Lee JW, Shim SH, Lee C. Controlled growth of SnO2 nanorods by thermal evaporation of Sn powders. J. Korean Phys Soc 2007;51:198–203.
[46] Al-Nasiry S, Geusens N, Hanssens M, Luyten C, Pijnenborg R. The use of Alamar Blue assay for quantitative analysis of viability, migration and invasion of choriocarcinoma cells. Hum Reprod 2007;22:1304–9.
[47] Räz B, Iten M, Grether-Bühler Y, Kaminsky R, Brun R. The Alamar Blue® assay to determine drug sensitivity of African trypanosomes (Tb rhodesiense and Tb gambiense) in vitro. Acta Tropica 1997;68:139–47.
[48] Rampersad SN. Multiple applications of alamar blue as an indicator of metabolic function and cellular health in cell viability bioassays. Sensors 2012:12347–60. doi: https://doi.org/10.3390/s120912347.
[49] Fu F, Gu J, Cao J, Shen R, Liu H, Zhang Y, et al. Reduction of silver ions using an alkaline cellulose dope: straightforward access to Ag/ZnO decorated cellulose nanocomposite film with enhanced antibacterial activities. ACS Sustain Chem Eng 2017;6:738–48.
[50] Sinha T, Ahmaruzzaman M, Adhikari PP, Bora R. Green and environmentally sustainable fabrication of Ag-SnO2 nanocomposite and its multifunctional efficacy as photocatalyst and antibacterial and antioxidant agent. ACS Sustain Chem Eng 2017;5:4645–55.
[51] Yalcinkaya F, Lubasova D. Quantitative evaluation of antibacterial activities of nanoparticles (ZnO, TiO2, ZnO/TiO2, SnO2, CuO, ZrO2, and AgNO3) incorporated into polyvinyl butyral nanofibers. Polym Adv Technol 2017;28:137–40.
[52] Avi-Dor Y, Kuczynski M, Schatzberg G, Mager J. Turbidity changes in bacterial suspensions: kinetics and relation to metabolic state. Microbiology 1956;14:76–83.
[53] Hajipour MJ, Fromm KM, Ashkarran AA, de Aberasturi DJ, de Larramendi IR, Rojo T, et al. Antibacterial properties of nanoparticles. Trends Biotechnol 2012;30:499–511. doi: https://doi.org/10.1016/j.tibtech.2012.06.004.

Eduardo B. Tibayan Jr obtained PhD from Department of Physics, De La Salle University, Manila and currently he serves as dean at the College of Humanities and Sciences, De La Salle Health Sciences Institute, Dasmariñas City, Cavite, Philippines.

Muhammad Akhsin Muflikhun currently as a PhD student from the Department of Aeronautics and Astronautics, The University of Tokyo. He is a permanent lecturer from department of mechanical and industrial engineering, Gadjah Mada University, Indonesia. He obtained his master degree in the department of mechanical engineering, De La Salle University, Manila

Vipin Kumar obtained PhD from department of aeronautics and astronautics engineering, The University of Tokyo, Japan. Currently his position is a researcher at Manufacturing Demonstration Facility (MDF), Oak Ridge National Laboratory (ORNL), Knoxville, TN, 37932, USA

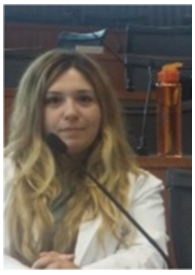

Christine Fisher works as researcher in the Chemical Sciences Division (CSD), Oak Ridge National Laboratory (ORNL), Oak Ridge, TN, 37830, USA. She obtained PhD from City University of New York-College of Staten Island.

Al Rey C. Villagracia serve as Research Unit Head, Advanced Nanomaterials Investigation by Molecular Simulations (ANIMoS) De La Salle University, Manila. He obtained his PhD in the Department of Physics, De La Salle University, Manila

Gil Nonato C. Santos is a full professor from the Department of Physics, De La Salle University, Manila. Currently he serves as a Vice Chancellor at De La Salle University Laguna Campus. He also serves as a head of iNano research facility, De La Salle University, Manila.